Journal of Petroleum Research and Studies

Open Access
Vol. 15, No. 1, March 2025, pp. 197-210

P- ISSN: 2220-5381
E- ISSN: 2710-1096

DOI: http://doi.org/10.52716/jprs.v15i1.898

Effect of Strontium on the Structural, Optical, and Magnetic Properties of $Bi_{(1-x)}Sr_xFeO_3$

Khalid H. Jebur
Ministry of Oil, Baghdad Oil Training Institute, Baghdad, Iraq.
Corresponding Author E-mail: khaled7005b.rrrrrtrtttrrrrrr@gmail.com

Received 02/01/2024, Revised 17/03/2024, Accepted 28/03/2024, Published 21/03/2025

Abstract

The composite Bi(1-x) SrxFeO$_3$ ($x = 0.0, 0.2, 0.4, 0.6, 0.8$) was produced via solid-state reaction technique at 850 °C, in order to evaluate how strontium affects the structure. X-ray diffraction (XRD), scanning electron microscopy (SEM), energy-dispersive X-ray spectroscopy (EDX), magnetic analysis (VSM), and band gap energy measurements were performed by UV- visible spectroscopy. The results obtained are the formation of crystalline materials of rhombohedral surfaces and change to the pseudocubic phase at $x = 0.4$. The particle size declines from 36.5 nm up to 17 nm for the pure sample in BSFO. The strontium Sr+2 caused an increase in Remnant magnetization (Mr) and coercive field (Hc), which lead to the magnetization development of BiFeO3, UV- visible spectroscopy used to calculate the direct optical band gap of all samples had its value on the order of 2.4 to 2.9 eV.

Keywords: solid-state reaction, Bi$_{(1-x)}$SrxFeO$_3$, magnetic properties.

تأثير السترونتيوم على الخواص البنيوية والبصرية والمغناطيسية لـ $Bi_{(1-x)}Sr_xFeO_3$

الخلاصة:

تم إنتاج المركب $Bi_{(1-x)}Sr_xFeO_3$ ($x = 0.0, 0.2, 0.4, 0.6, 0.8$) عبر تقنية تفاعل الحالة الصلبة عند 850 درجة مئوية، لتقييم كيفية تأثير السترونتيوم على البنية. تم إجراء حيود الأشعة السينية (XRD)، المجهر الإلكتروني الماسح (SEM)، التحليل الطيفي للأشعة السينية المشتتة من الطاقة (EDX)، التحليل المغناطيسي (VSM)، وقياسات فجوة النطاق بواسطة التحليل الطيفي للأشعة فوق البنفسجية المرئية. النتائج المتحصل عليها هي تكوين مواد بلورية ذات سطوح معينية الشكل وتحولها إلى الطور الكاذب عند $x = 0.4$. ينخفض حجم الجسيمات من 36.5 نانومتر حتى 17 نانومتر للعينة النقية في BSFO. تسبب السترونتيوم Sr+2 في زيادة مغنطة البقايا (Mr) والمجال القسري (Hc)، مما أدى إلى تطوير مغنطة $BiFeO_3$، ويستخدم التحليل الطيفي للأشعة فوق البنفسجية المرئية لحساب التأثير البصري المباشر فجوة النطاق لجميع العينات كانت قيمتها في حدود 2.4 إلى 2.9 الكترون فولت.

1. Introduction

The field of studies on multiferroic (MF) materials has advanced significantly in the past few years the main reasons for this are the small-temperature magnetic stage transition in materials that were not ferroelectric in their non-magnetically ordered form, the appearance of electric polarization, and the discovery of magneto-electric coupling [1]. These materials' low temperatures at which these phenomena are detected and their weak magnetic/electric polarization make them inapplicable, despite the great interest non understanding the fundamentals of multiferroic features. Potentially coupling electric and magnetic polarizations could offer an extra degree of flexibility for device design and applications, such the rapidly developing field of spintronics [2], multiple state memory elements, [3] electric field controlled ferromagnetic resonance devices and transducers with magnetically moderated piezoelectricity [4]. Amid all multiferroic materials studied so far, ABO_3-type perovskite structure $BiFeO_3$ (BFO) is a known Pb-free and environmentally approachable material. $BiFeO_3$ is ferroelectric (Curie temperature $T_C = 1100$ K), antiferromagnetic (Neel point $T_N = 643$ K). BFO has a rhombohedral distorted structure (space group R3c), shows G-type antiferromagnetic, and at room temperature has mild magnetic. Both big crystals and thin films can be made with it [5]. Apart from the possible uses as a magnetoelectric material, BFO film could also be employed as a photocatalytic material [6] and because of its tiny bandgap (Eg = 2.5 eV) in ultrafast optoelectronic devices [7]. The long-range ordering caused by the presence of the Bi lone pair and the hybridization between the Bi 6s and 2p orbitals is the fundamental source of the ferroelectricity mechanism [7, 8].

The magnetic order resulting from the super exchange interaction is caused by the Fe ion [8]. One major barrier to the actual usage of BFO is its antiferromagnetic character [5]. Elements in the periodic table are trivalent (La3+, Eu3+, Nd3+, or Sm3+) A-site replacements [9] cations for Bi3+ and B-site replacements for Fe3+ made by donors [10]. However, a number of studies have reported on how divalent ion doping (Ca2+, Sr2+, Pb2+, and Ba2+) might alter the magnetic or dielectric characteristics of BFO [11]. The choice of Sr is more intriguing than other divalent substituents in light of the recent investigation on $Bi_{0.8}Sr_{0.2}FeO_{3}$-δ samples, since the magnetic field-induced polarization (Pr = 96 $\mu C/cm^2$ at 10 T) is among the highest recorded for BFO based systems in either thin film or bulk forms [12]. The magnetic and ferroelectric properties of $Bi_{1-x}Sr_xFeO_3$ were studied with regard to the function of the Fe oxidation state (Iron ion Fe^{2+}, Iron ion Fe^{3+}, and Iron ion Fe^{4+}), and it was demonstrated that Fe ions in this compound displayed Fe^{2+} and

Fe^{5+} states. On the other hand, Li et al. [13] discovered that Fe ions remained in a Fe^{+3} state and that the samples' magnetism dropped as the Sr content increased. They ascribed this to the reduction in Fe^{3+} coordination from an octahedral to a tetrahedral form. The research aims to prepare $Bi_{(1-x)}Sr_xFeO_3$ compounds using the solid-state reaction method in different strontium proportions ($x = 0.0, 0.2, 0.4, 0.6, 0.8$), and study the structural, magnetic and electrical properties of the prepared samples .

2. Experimental work

2.1 Materials:

A collection of single phase models of $Bi_{1-x}Sr_xFeO_3$ of $x = 0.0, 0.2, 0.4, 0.6$, and 0.8 were created through conventional solid state reaction technique using powders of pure Bi_2O_3 (99.9%), $SrCO_3$ (99.9%) and Fe_2O_3 (99.8%) in their stoichiometric ratio [14] According to the following equation:

$$SrCO_3 + Fe_2O_3 + Bi_2O_3 \rightarrow Sr\,Bi_2\,Fe_2\,O_3 + CO_2$$

We grind the samples to obtain a fine powder, then the mixture is inserted into an Alumina crucible to obtain a pure phase after heating the mixture to 800°C. Many published research often claim the $BiSrFeO_9$ phase as not produced [15]. The samples were palletized into discs with a diameter of 10 mm and a thickness of 3–4 mm using a pressure of 5 tons ($98 \times 10^5 \frac{N}{m^2}$). After four hours of annealing at 850°C, the pellets were cooled to ambient temperature in the furnace.

2.2 Laboratory equipment used

X-ray diffraction (XRD), scanning electron microscope (SEM), energy dispersive X-ray spectroscopy (EDX), magnetic analysis (VSM), and band gap energy measurements by ultraviolet-visible spectroscopy were used to accomplish this research.

3. Results and Discussion

3.1 Structure characterization

Figure (1) shows the XRD pattern of $Bi_{1-x}Sr_xFe_2O_3$. When $x = 0$, there are several distinct peaks under Bi_2O_3 and matched with the global card (JCPDS 00-045- 1344). While the yaw angle at 43^0 corresponds to the iron shear level (110) and corresponds to the card (JCPDS 00-003-1050) [16]. The average crystal size of $Bi_{1-x}Sr_xFe_2O_3$ at $x = 0$ is about 36.5 nm. The value of Sr is zero, so no peaks due to Sr nanoparticles. Figure (2), XRD pattern of $Bi_{1-x}Sr_xFe_2O_3$ when $x = 0.2$, in these samples the proportion of Bi decreased and the values of Sr are 0.2, there are some changes in behavior below the ratio Percentage of Sr nanoparticles, characteristic peak of strontium oxide bismuth corresponding to the card (JCPDS 00-046-0484). The average crystal size of $Bi_{0.8}Sr_{0.2}Fe_2O_3$ is about 25.3 nm, and the crystal structure is cubic [17]. While the other diffraction angles below are for bismuth iron oxide and correspond to the card JCPDS 00-014-0181.

Figure (3) shows the XRD pattern of $Bi_{1-x}Sr_xFe_2O_3$ when x = 0.4. The percentage increase in Sr changes the structure and behavior of nanomaterials, therefore, the intensity of the diffraction angles has been changed, and the Sr pattern can be distinguished from the diffraction angles at 29 degrees and corresponding to the plane (110). These data agree with the card Standard (JCPDS 0484-046-00). While this other diffraction peak with some variation agrees with Fe_2O_3 and Bi_2O_3. The mean crystal size of $Bi_{0.6}Sr_{0.4}Fe_2O_3$ has been estimated to be around 22.5 nm.

Figure (4) indicates the XRD pattern of $Bi_0.4Sr0.6Fe2O_3$ at (x= 0.6). The strongest peak at a diffraction angle of 32° corresponding to the plane (-110) is shown and matched to the card Standard JCPDS 01-074-2493, the behavior is consistent with the iron oxide nanocomposite of bismuth where the rhombic shape is determined. The average crystal size of $Bi_{0.4}Sr0_{.6}Fe2O_3$ was calculated to be 22.2 nm. Figure (5) shows the XRD pattern of $Bi_{1-x}Sr_xFe_2O_3$ when x = 0.8, and the high crystallinity appears homogeneously when the percentage of Sr = 0.8. They agree very well with the card standard JCPDS 01-082-2327 and refer to the strontium-bismuth iron oxide nanocomposite and the crystal shape is cubic.

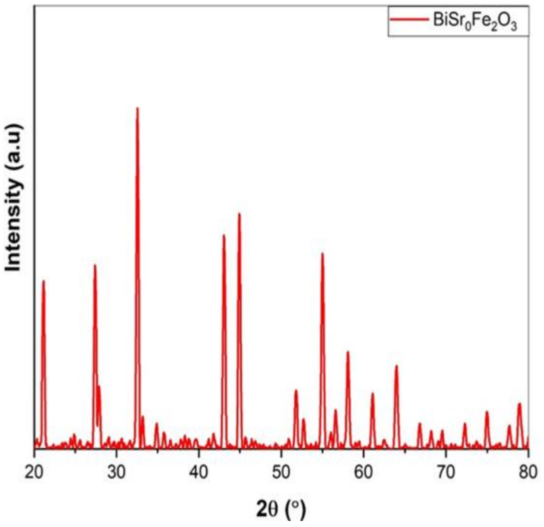

Fig. (1): XRD pattern of $Bi_{1-x}Sr_xFe_2O_3$, when x=0

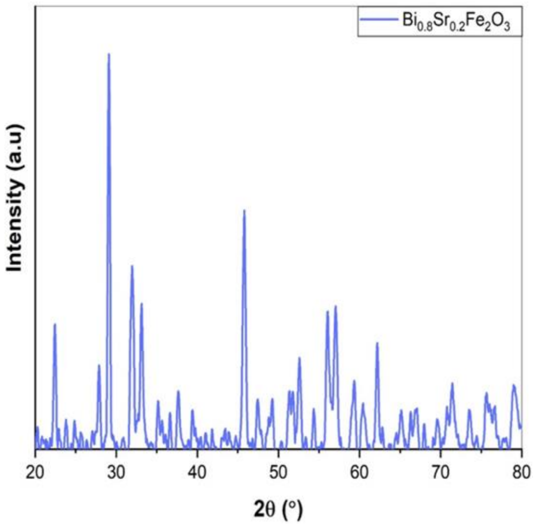

Fig. (2): XRD pattern of $Bi_{1-x}Sr_xFe_2O_3$, when x=0.2

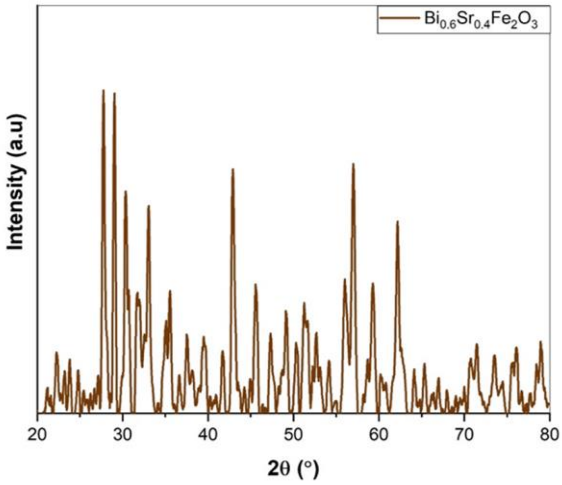

Fig. (3): XRD pattern of $Bi_{x-1}Sr_xFe_2O_3$, when x=0.4

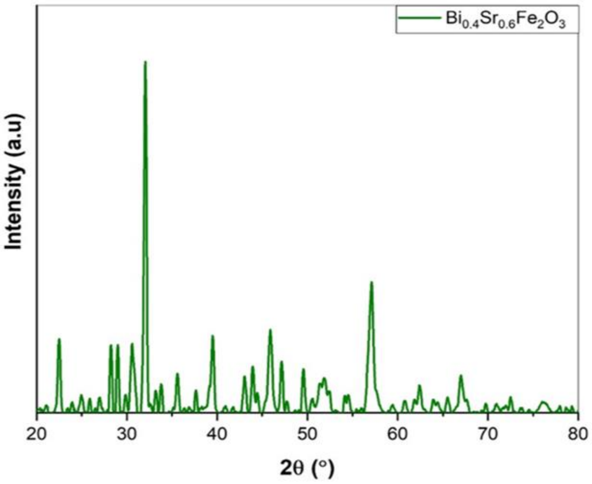

Fig. (4): XRD pattern of $Bi_{1-x}Sr_xFe_2O_3$, when x=0.6

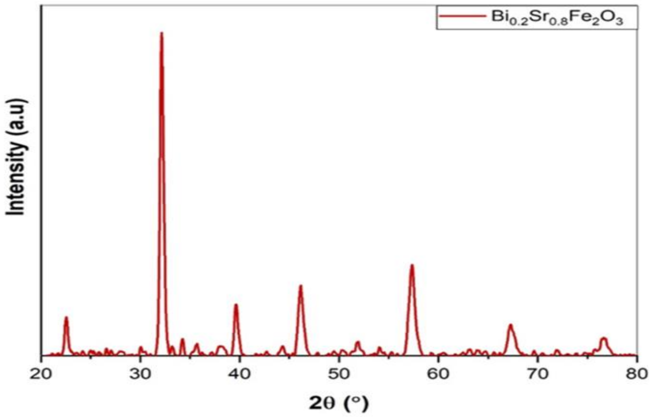

Fig. (5): XRD pattern of $Bi_{1-x}Sr_xFe_2O_3$, when x=0.8

The optical absorption for semiconductor material can determine the energy band gap. The diffuse reflectance spectra were collected and converted into absorption spectra using the Tauc Plot method.

$$\alpha h\nu = A\,(h\nu - E_g)^{n/2} \qquad \ldots\ldots\ldots\ldots\ldots\ldots\ldots\ldots\ldots\ldots\ldots\ldots\ldots\ldots\ldots\ldots\ldots\ldots\ldots\ldots\ldots\ldots(1)$$

(α) is the absorption coefficient, (hυ) is the energy, (B) is a constant equal to 1, (Eg) is the energy gap, and n is the electronic transition.

The band gap was drawn by extrapolating the linear area of chart $(h\nu\ \alpha)^2$ on the Y-axis against the energy on the X-axis, and the result was according to Figures (6), (7), (8), (9), and (10) that the energy gap increases with the increase in the added rates. This is due to the fact that increasing the added rates will lead to a decrease in the energy levels, which leads to the fusion of the molecules, the particle size becomes smaller, and thus the energy gap increases.

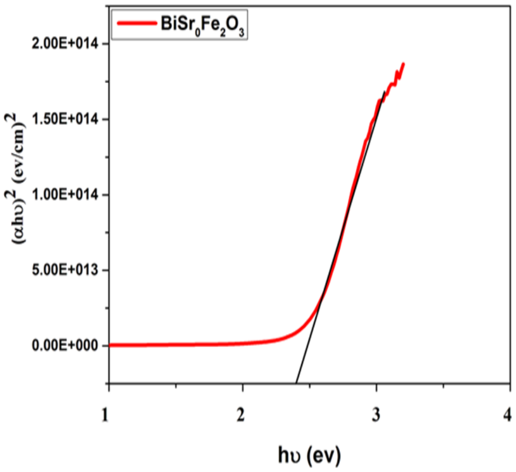

Fig. (6): Band gapfor $Bi_{(1-x)}Sr_xFe_2O_3$at X=0

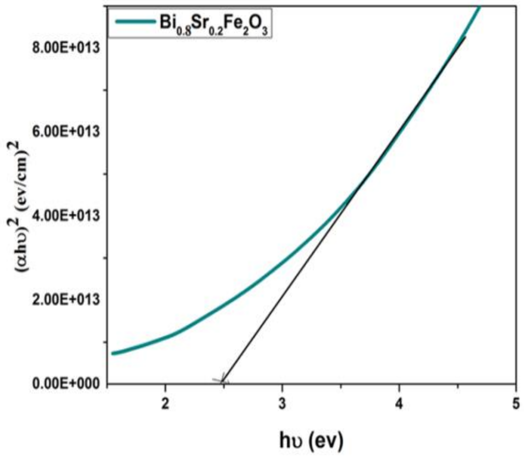

Fig. (7): Band gap for $Bi_{(1-x)}Sr_xFe_2O_3$ at X=02.

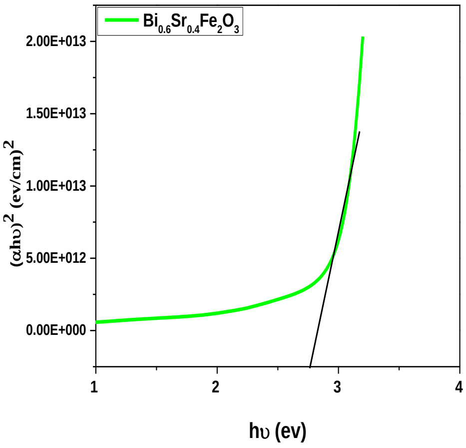

Fig. (8): Band gap for $Bi_{(1-x)}$ Sr_x Fe_2O_3 at X=0.4

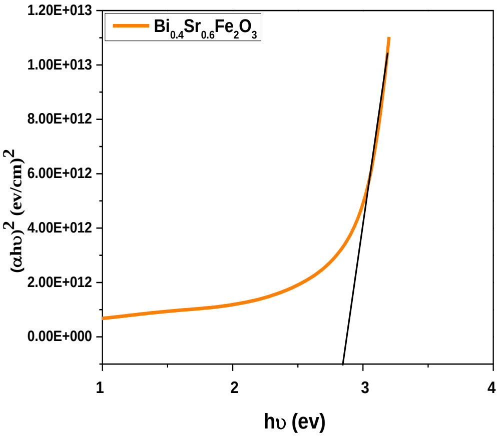

Fig. (9): Band gap for $Bi_{(1-x)}$ Sr_x Fe_2O_3 at X=0.6

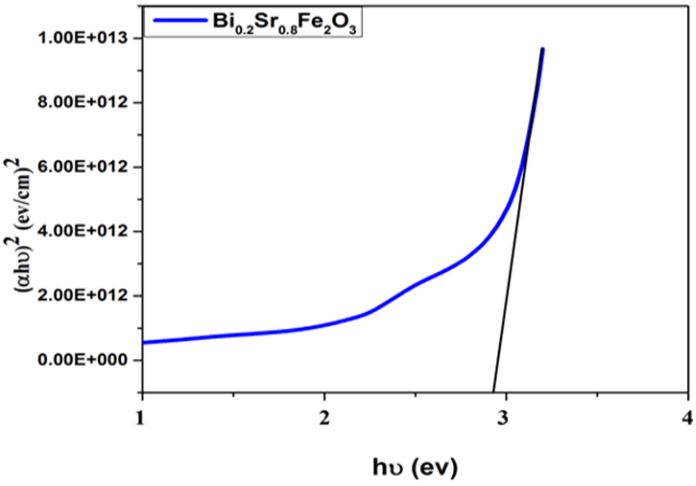

Fig. (10): band gap for $Bi_{(1-x)}$ Sr_x Fe_2O_3 at X=0.8

3.2 Scanning electron microscopy (SEM) and (EDX)

The morphology of the prepared sample was determined by SEM and EDx at different magnifications and is shown in Figures (11, 12, 13, 14, and 15). The SEM images clearly reveal that BFO powder show pores or voids with different size and shape (Figure 11 a), in addition to the presence of agglomerate and nonhomogenous particles (Figure 11b).

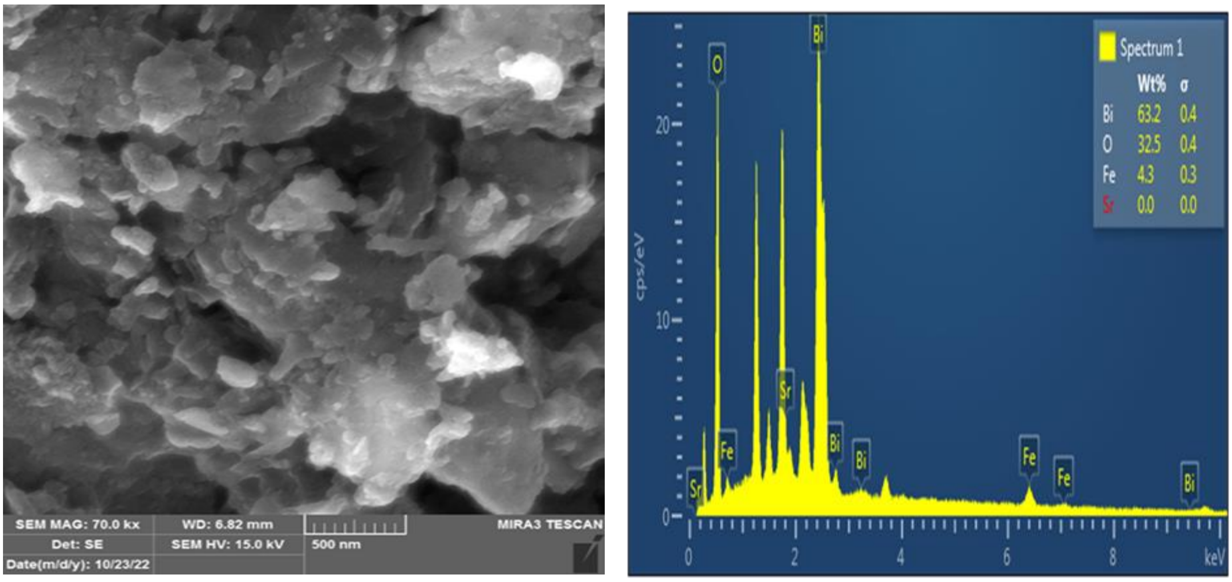

Fig. (11 a and b): The FESEM and EDx images of BiSr Fe_2O_3 , x=0

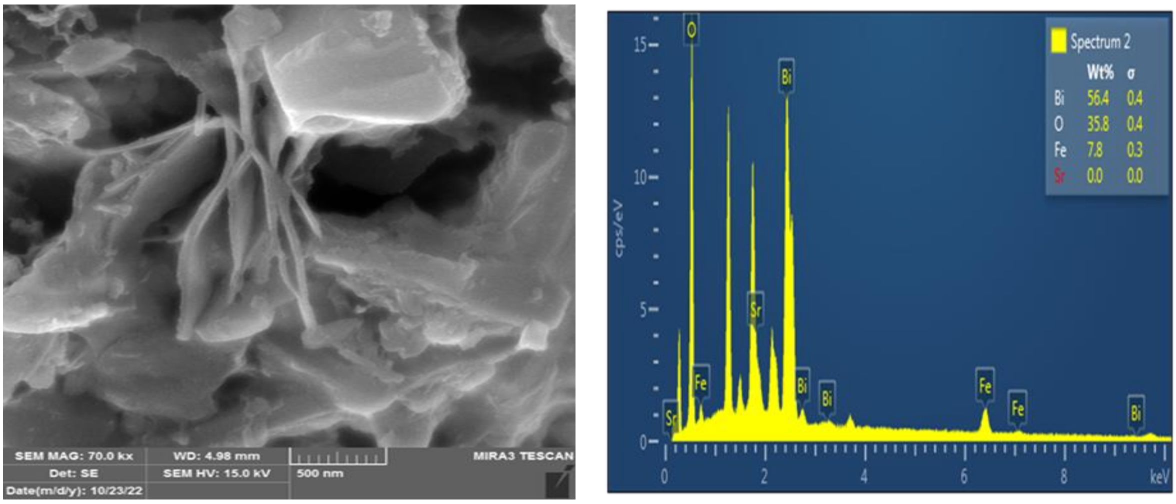

Fig. (12 a and b): The FESEM and EDx images of $Bi_{0.8}Sr_{0.2}Fe_2O_3$ with x=0.2

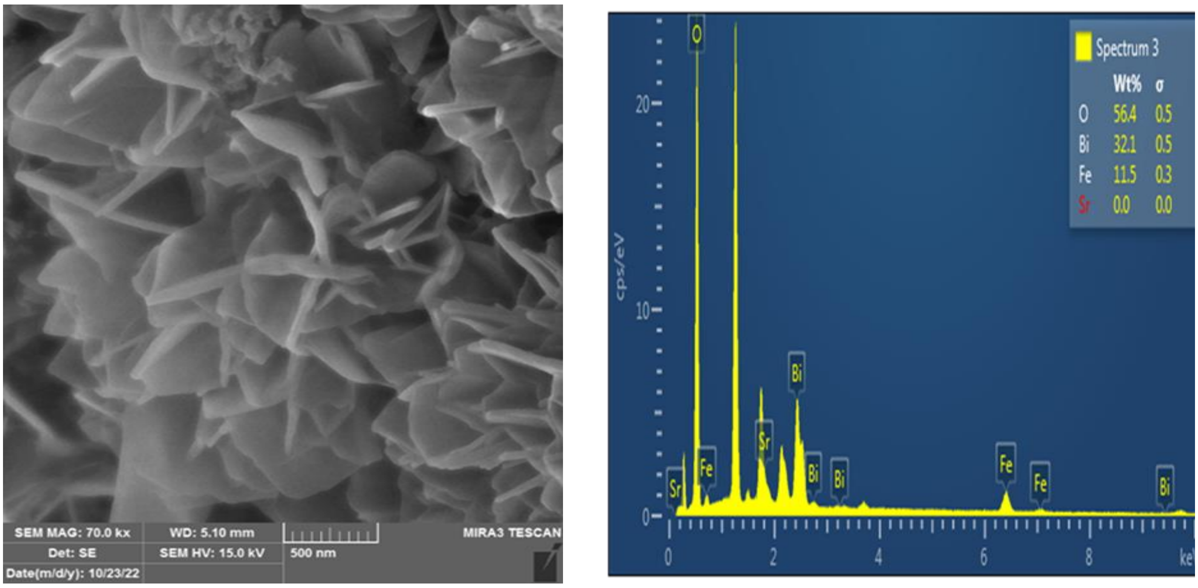

Fig. (13 a, b and c): The FESEM and EDx images of $Bi_{0.6}Sr_{0.4}Fe_2O_3$ with x=0.4

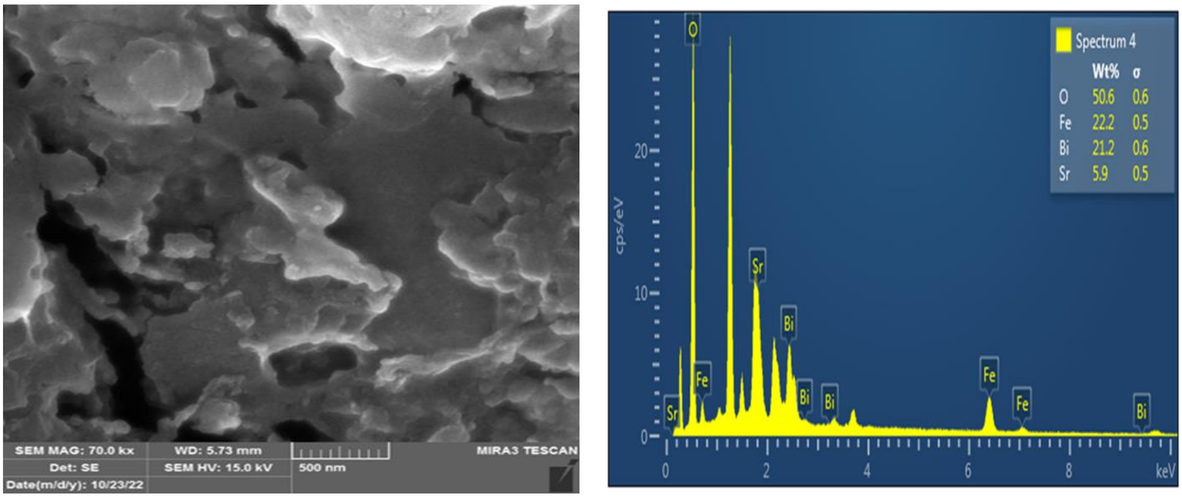

Fig. (14 a and b): The FESEM and EDx images of $Bi_{0.4}$ $Sr_{0.6}$ Fe_2O_3 with x=0.6

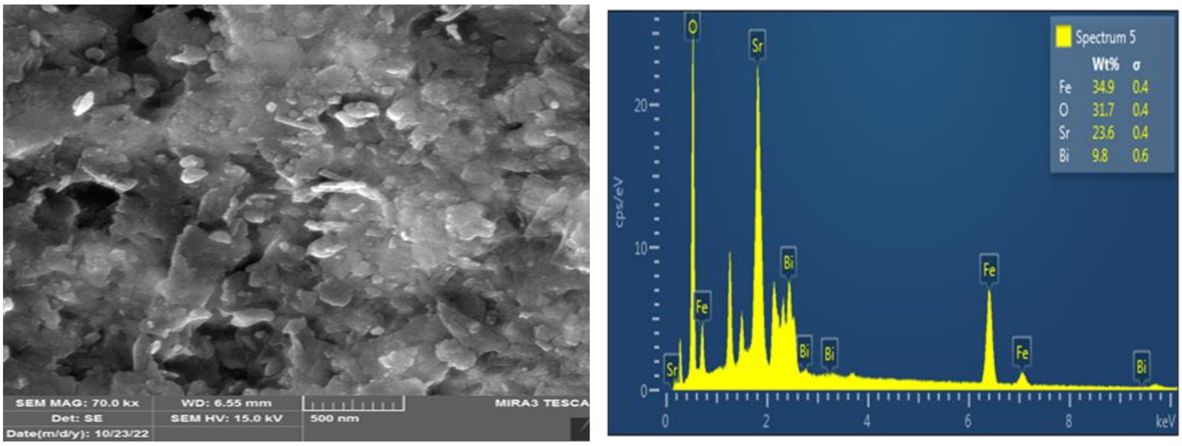

Fig. (15 a and b): The FESEM and EDx images of $Bi_{0.2}$ $Sr_{0.8}$ Fe_2O_3 with x=0.8

The percentage of Sr NPs is an important parameter for controlling the shape and morphology of materials and strongly depends on the shape change on the x value. The figures show that the morphology of $BiSr_xFe_2O_3$ when increasing the value of x, means that the percentage of Sr NPs increases and decreases in Bi NPs, as a result of the corresponding Edx there is a total change in shape because it was irregular.

3.3 Magnetic properties

The difference in the magnetic moment regularized to the models in (emu/gm) as a function of the applied magnetic field (H) at a fixed temperature, i.e. T= 300 K, for models of ($0.2 \leq x \leq 0.8$) are shown in Figure (16) and the derived magnetic parameters are abridged in Table (1). It is widely acknowledged that BFO_3 is a G-type antiferromagnetic material with linear magnetic field dependence of magnetization in the magnetic hysteresis loop. The magnetic response observed for as-synthesized nanoparticles of $Bi_{1-x}Sr_xFeO_3$ exhibits improved magnetization as exposed in Figure (17). arguing that with increasing diamagnetic doping of Sr^{2+}, the spiral spin structure of $BiFeO_3$ is repressed and, on the other hand, the polarized moment of Fe is enhanced, i.e., ferromagnetic order is enhanced, and it may be abolished totally for x = 0.4. Consequently, the residual magnetization Mr values exhibit a progressive increase, culminating in a maximum value of Mr = 18.51 emu/g for x = 0.8. There could be several explanations for the observed magnetic behavior. One possibility is that portion of the Fe^{3+} ions in the BFO will transform into Fe^{4+} ions as the concentration of divalent Sr^{2+} ions (diamagnetic material) increases at the Bi-site. Because of this substitution, there is a greater chance that some oxygen vacancies will exist in order to offset the charge of the doped BFO models. It follows that in order to offset the charge imbalance caused by doping Sr^{2+} ions rather than Bi^{3+} ions, oxygen vacancies must have been introduced into the material. Furthermore, Fe^{3+}–O–Fe^{3+} chains exhibit antiferromagnetic behavior in pure BFO, (Figure 18). Furthermore, demonstrated that the presence of oxygen vacancies causes the Fe^{3+} –O–Fe^{3+} bond angle to grow, the Fe^{3+} ions' spin to be canted, and net magnetization to be generated. As Sr^{2+} ion doping concentration rises, more oxygen vacancies are produced, and the bond angle of Fe^{3+}–O–Fe^{3+} keeps growing, both of which contribute to an increase in magnetism. As a result, more spins are canted, which boosts the magnetization. These findings concur with ours. The ionic radii of the doped element may also be a significant influence in increasing the net magnetization of $BiFeO_3$, independently of oxygen vacancies in the $Bi_{1-x}Sr_xFeO_3$ series. The doping element's ionic radius needs to be higher than the ionic radius of Bi^{3+}. The larger ionic radii of the doped element suppresses the spiral spin structure and the inversion symmetry is broken. In doped $BiFeO_3$, the structure is altered to a cycloidal type structure, and net magnetization is induced. Additionally, due of the increased spin canting at the particle surface, the greater surface-to-volume ratio of nanoparticles may enhance the magnetization [18].

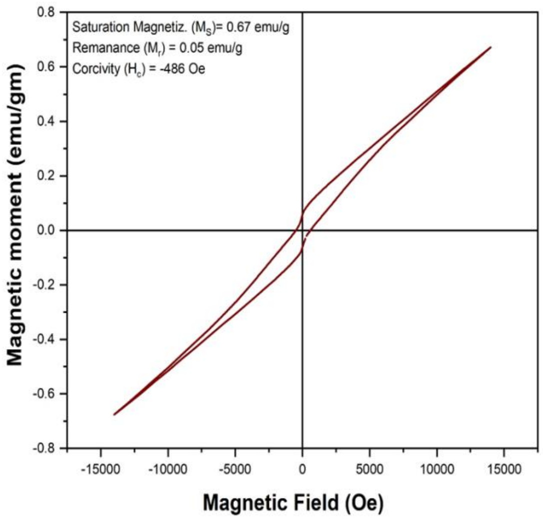

Fig. (16): The VSM graph of BiSr0Fe2O3 with x=0

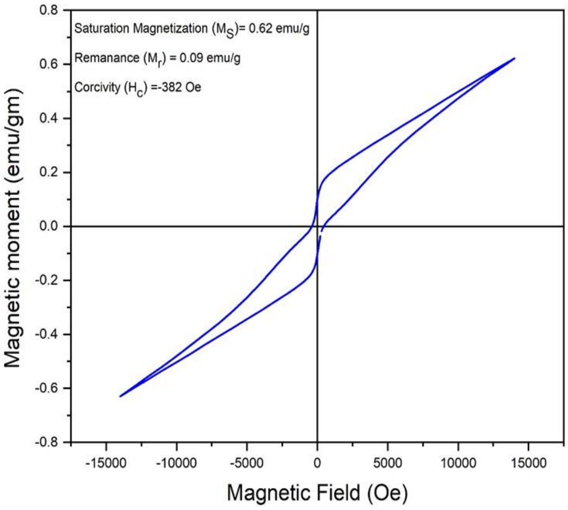

Fig. (17): The VSM graph of $Bi_{0.8}Sr_{0.2}$ Fe_2O_3 with x=0.2

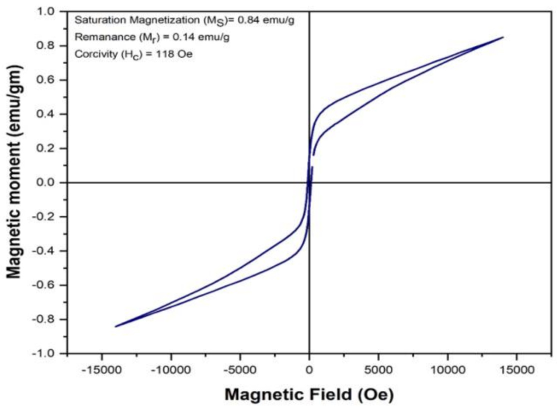

Fig. (18): The VSM graph of $Bi_{0.6}Sr_{0.4}$ Fe_2O_3 with x=0.4

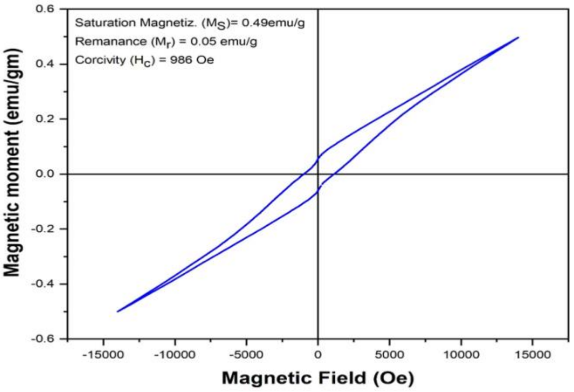

Fig. (19): The VSM graph of $Bi_{0.4}Sr_{0.6}$ Fe_2O_3 with x=0.6

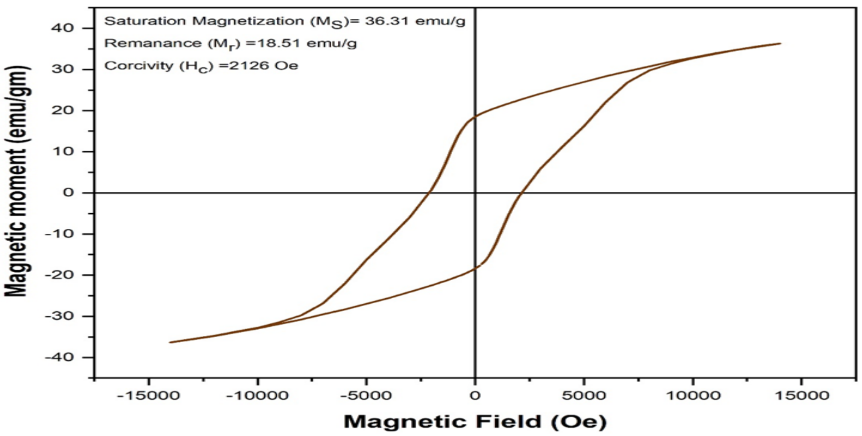

Fig. (20): The VSM graph of $Bi_{0.2}Sr_{0.8}$ Fe_2O_3 with x=0.8

Table (1): Results of magnetic measurements

Sample	Saturation magnetization M_S (emu/gr)	Residual magnetization M_T (emu/gr)	Coercive field H_C (Oe)
X=0	0.67	0.05	486
X=0.2	0.62	0.09	382
X=0.4	0.84	0.14	118
X=0.6	0.49	0.05	986
X=0.8	36.31	18.51	2126

4. Conclusions

Based on the calculated magnetic characteristics, it can be said that Sr doping improves BFO's magnetization, but as the doping level rises over x = 0.4, the second phase forms and the BFO's magnetization deteriorates.

In this work Sr substituted $Bi_{1-x}Sr_xFeO_3$ has prepared by the solid-state reaction technique and for four hours, the produced samples were sintered at 850 °C. Utilizing the X-ray diffraction technique (XRD), the microstructural properties were examined. The perovskite structure with Phase group R3c is confirmed by XRD analysis of the produced materials. The average size of a crystallite was calculated using the Sherrer formula, and it is between 37 and 17 nm. This substance is particularly useful for technological applications because of the morphological outcomes that doping clarifies.

We note that with the increase in the concentration of the additive, the particle size of the compound will decrease, and we note that the shape of the compound is irregular and slightly crystalline. Crystallinity increases with an increasing ratio. The optical energy gap increases with the increase in the concentration of the additive. We note from the magnetic measurements that the composite shows soft behavior when Sr concentration = 0 and the behavior turns hard with increasing Sr concentration.

References:

[1] S. Sindhu, and M. R. Anantharaman, "Preparation and Characterization of Spinel Ferrites –Their Incorporation in Rubber Matrix and Evaluation of Properties," *PhD diss., Cochin University of Science and Technology*, 2001. http://dyuthi.cusat.ac.in/purl/1001

[2] D. Dimos, and C. Mueller, "Perovskite Thin Films For High-Frequency Capacitor Applications", *Annual Review of Materials Research*, vol. 28, pp. 397-419, 1998. https://doi.org/10.1146/annurev.matsci.28.1.397

[3] A. I. Kingon, S. K. Streiffer, C. Basceri, and S. R. Summerfelt, "High-Permittivity Perovskite Thin Films for Dynamic Random-Access Memories", *MRS Bulletin*, vol. 21, no. 7, pp. 46-52, 1996. https://doi.org/10.1557/S0883769400035910

[4] H. Obayashi, Y. Sakurai, and T. Gejo, "Perovskite-type oxides as ethanol sensors", *Journal of Solid State Chemistry*, .vol17, no. 3, pp. 299-303, 1976. https://doi.org/10.1016/0022-4596(76)90135-3

[5] T. Rogers-Hayden and N. Pidgeon, "Moving engagemen, upstream" Nanotechnologies and the royal society and royal academy of engineering's inquiry," *Public Underst. Sci.*, vol. 16, no. 3, pp. 345–364, Jul. 2007. https://doi.org/10.1177/0963662506076141

[6] J. Wu, S. Mao, Z.-Guang Ye, Z. Xiea and L. Zhenga," Room-temperature ferromagnetic/ferroelectric BiFeO3 synthesized by a self-catalyzed fast reaction process", *Journal of Materials Chemistry*, vol. 20, no. 48, pp. 6512-6516, 2012. http://dx.doi.org/10.1039/C0JM00729C

[7] S. Gulah and L. Masoudi, "Study of the structural, electronic and magnetic properties of $BiFeO_3$ perovskite", *MA thesis, Al-Arabi Al-Tepsi University*.

[8] Y. F. Popov, A. K. Zvezdin, G. P. Vorob'Ev, A. M. Kadomtseva, V. A. Murashev, D. N. Rakov, D. Parsons, "linear magnetoelectric effect and phase transitions in bismuth ferrite, BiFeO3" , *JETP Letters*, vol 57, no. 1, pp. 69-73, 1993.

[9] N. A. Hill, "Why Are There so Few Magnetic Ferroelectrics?", *The Journal of Physical Chemistry B*, vol. 104, no. 29, pp. 6694-6709, 2000. https://doi.org/10.1021/jp000114x

[10] M. Amin, "Exploring the Multifunctional Properties of BiFeO3 -Based Multiferroics", *Department of Physics, University of the Punjab*, Lahore, 54590 (Pakistan), 2018.

[11] W. Nan, L. Xudong, L. Han, Z. Zhiqiang, R. Zhang, H. Olin, and Y. Yang, "Structure, Performance, and Application of $BiFeO_3$ Nanomaterials", *Nano-Micro Letters*, vol. 12, article no. 81, 2020. https://doi.org/10.1007/s40820-020-00420-6

[12] V. A. Khomchenko, D. A. Kiselev, J. M. Vieira, A. L. Kholkin, M. A. Sá, and Y. G. Pogorelov, "Synthesis and multiferroic properties of $Bi_{0.8}A_{0.2}FeO_3$ (A=Ca, Sr, Pb) ceramics", *Appl. Phys. Lett.*, vol. 90, no. 24, p. 242901, 2007. https://doi.org/10.1063/1.2747665

[13] A. Z. Simões, F. G. Garcia, and C. dos Santos Riccardi, "Rietveld analysys and electrical properties of lanthanum doped $BiFeO_3$ ceramics", *Materials Chemistry and Physics*, vol. 116, no. 2–3, pp. 305-309, 2009 .https://doi.org/10.1016/j.matchemphys.2009.04.036

[14] M. A. Awad, "Study the structural electrical and magnetic properties of M-type nano hexaferrites prepared via chemical route", *the Degree of master of the University of Kirkuk*, 2021.

[15] S. Palomares-Sánchez, S. Ponce-Castañeda, F. Ruiz, M. Mirabal-García, J. R. Martínez, and S. Díaz-Castañón, "Structural and magnetic characterization of (Ba,Sr)-hexaferrite powders," *Rev. Metal.*, vol. 35, no. 3, pp. 143–147, 1999. https://doi.org/10.3989/revmetalm.1999.v35.i3.617

[16] M. Troemel, "Institute für Anorganische Chemie der Johann Wolfgang", ICDD Grant-in-Aid Recipients, *Goethe-Universität*, Frankfurt, Germany, 2014.

[17] K. Uchino, S. Nomura, L. E. Cross, R. E. Newnham, and S. J. Jang, "Electrostrictive effect in perovskites and its transducer applications", *Journal of Materials Science*, vol. 16, pp. 569–578, 1981. https://doi.org/10.1007/BF00552193

[18] M. Z. Shoushtari, A. Emami, and S. E. M. Ghahfarokhi, "Effect of bismuth doping on the structural and magnetic properties of zinc-ferrite nanoparticles prepared by a microwave combustion method", *Journal of Magnetism and Magnetic Materials*, vol. 419, pp. 572-579, 2016. https://doi.org/10.1016/j.jmmm.2016.06.080